reactions

MDPI

Article

Combining Kinetics and In Silico Approaches to Evaluate Lipophilic Piperic Acid Esters as Anti-*Rhizopus oryzae* Lipase Agents for Olive Oil Preservation

Amira Mahfoudhi [1], Nidhal Tarhouni [2], Othman A. Alghamdi [3], Ahmed Fendri [4] and Adel Sayari [1,3,*]

[1] Laboratory of Biochemistry and Enzymatic Engineering of Lipases, Engineering National School of Sfax (ENIS), University of Sfax, Sfax 3038, Tunisia; amira.mahfoudhi95@gmail.com
[2] Laboratory of Enzyme Engineering and Microbiology, Engineering National School of Sfax (ENIS), University of Sfax, Sfax 3038, Tunisia
[3] Department of Biological Sciences, College of Science, University of Jeddah, Jeddah 23890, Saudi Arabia
[4] Laboratory of Molecular and Functional Genetics, Faculty of Science, University of Sfax, Sfax 3038, Tunisia
* Correspondence: aasayari@uj.edu.sa or adelsayari3@gmail.com

Abstract

Rhizopus oryzae lipase (ROL) is a key enzyme involved in olive oil spoilage and acts as a virulence factor in fungal infections. Natural lipophilic lipase inhibitors are crucial for mitigating economic losses resulting from lipid degradation in stored or decaying olive fruits. This study evaluated a series of enzymatically synthesized piperate esters with varying alkyl chain lengths (butyryl, C4; octyl, C8; dodecyl, C12) for their inhibitory effects on ROL activity. Octyl piperate (C8) demonstrated the highest potency, with IC_{50} values of 0.05 mg/mL using methods B and C or 0.25 mg/mL using method A. Molecular docking indicated that C8 achieved the most favorable predicted binding energy (Gscore: –11.134 kcal/mol), primarily through hydrophobic interactions (Val329, Ala212, Phe209) and hydrogen bonds with oxyanion hole residues (Ser268, Thr206, Gln241). Molecular dynamics simulations confirmed that C8 maintained stable binding and stabilized the catalytic residues. In comparison, C4 exhibited weaker interactions, and the longer C12 chain induced conformational instability and steric hindrance. These results establish a parabolic structure–activity relationship, identifying the octyl chain (C8) as optimal for ROL inhibition among the tested derivatives. The rational design of lipophilic, biodegradable lipase inhibitors thus positions octyl piperate as a promising candidate for extending olive storage and shelf life, and as a scaffold for developing natural antifungal agents targeting virulent *R. oryzae* strains.

Keywords: *Rhizopus oryzae* lipase inhibition; lipophilic piperic acid esters; in vitro and in silico studies; structure-activity relationship

Check for updates

Academic Editor: Dmitry Yu. Murzin

Received: 1 February 2026
Revised: 4 March 2026
Accepted: 6 March 2026
Published: 11 March 2026

Copyright: © 2026 by the authors. Licensee MDPI, Basel, Switzerland. This article is an open access article distributed under the terms and conditions of the Creative Commons Attribution (CC BY) license.

1. Introduction

Fungal lipases are indispensable enzymes in industrial biotechnology, where they catalyze reactions ranging from biodiesel production to flavor development, as well as in pathogenic processes, where they facilitate tissue invasion and nutrient acquisition [1]. Consequently, the search for selective lipase inhibitors has become a vibrant research field. Natural products, especially plant-derived secondary metabolites [2], have emerged as a rich source of bioactive compounds that can modulate lipase activity without the drawbacks of synthetic chemicals. Polyphenols, flavonoids, terpenoids, phenylpropanoids, and alkaloids have demonstrated inhibitory effects against various fungal and mammalian lipases.

This activity translates into therapeutic benefits for disorders where lipase dysregulation is a significant factor, such as peptic ulcers, acne vulgaris [3,4], and obesity [4–6].

Various natural sources, such as marine algae [7], soybeans [8], wheat [9], citrus fruits [10], oolong tea [11], and medicinal herb extracts [12], contain compounds that inhibit lipase activity [13]. Despite these findings, identifying more potent and effective inhibitors remains a priority. Natural lipase inhibitors offer both a sustainable alternative for industrial oil preservation and potential leads for developing pharmacological agents targeting lipase-related diseases.

In this context, several classes of plant metabolites have shown notable lipase inhibitory activity. Saponins such as platycodin D [13], flavonoids like quercetin [14,15], and alkaloids including berberine and sanguinarine [16] have demonstrated significant effects. Among these bioactive compounds, piperic acid derivatives remain relatively understudied but represent a promising class of potential lipase inhibitors [17]. Piperic acid, a naturally occurring phenylpropanoid, possesses a conjugated diene system and a carboxylic acid moiety that can be chemically modified to enhance lipophilicity and enzyme affinity [18].

Rhizopus oryzae lipase is particularly significant in both biotechnology and medicine [1,19]. In addition to its widespread use in various biotechnological applications [20], it serves as a model enzyme for studying fungal pathogenic lipases. Inhibiting this enzyme could have important implications for managing *R. oryzae* strains that show resistance to conventional antifungal treatments.

Moreover, olive oil is prized for its sensory qualities and health-promoting fatty acids. Yet, its shelf life is limited by enzymatic hydrolysis, which generates free fatty acids and off flavors. The lipase produced by *Rhizopus oryzae* is a major contributor to this degradation and is a primary contaminant in rotting olives [19,21], particularly during the storage and processing of olives and olive-based products. Inhibiting this enzyme presents a promising strategy for enhancing olive oil stability without relying on synthetic chemicals, which can impact flavor or consumer acceptance [22]. Lipase inhibition results in reduced enzymatic hydrolysis of triglycerides in olive fruits, thereby slowing the onset of rancidity [22] and preserving the distinctive aromas and flavors that define high-quality olive oil. Ultimately, inhibiting this enzyme is crucial for maintaining the integrity and marketability of olive oil, particularly during storage and transport, where enzymatic activity can be triggered [21,23].

The synthesis of novel lipase inhibitors has traditionally relied on chemical methods involving harsh conditions. However, enzymatic synthesis offers a more sustainable alternative, enabling the production of target compounds under mild conditions with minimal environmental impact [24,25]. Notably, lipases are highly versatile catalysts capable of promoting various reactions, including hydrolysis, acidolysis, and esterification, across different media [26–29]. Their exceptional selectivity further enhances their value for precise synthetic applications [30].

Previous work established an efficient enzymatic method for synthesizing piperic acid derivatives [17]. This study investigates the inhibitory effects of these piperic acid esters on *R. oryzae* lipase using both in vitro and in silico approaches. Three inhibition assays were employed to assess their effectiveness, along with molecular docking to examine the binding mechanisms. The in-silico analyses specifically evaluated how ester carbon chain length affects binding affinity and interaction profiles within the lipase active site, aiming to clarify the structure-activity relationships of these compounds.

2. Materials and Methods

2.1. Preparation of Piperic Acid and Piperate Esters

Piperic acid was prepared by alkaline hydrolysis of piperine (the principal constituent of *P. nigrum*) according to a previously described protocol [31,32].

Lipophilic derivatives of piperic acid (butyl-, octyl-, and dodecyl-piperates) were enzymatically synthesized as described previously [17]. HPLC analysis using a C-18 column (250 × 4.6 mm) at 35 °C with a 60:40 acetonitrile:water mobile phase (1 mL/min, 30 min) [17] was used to detect the esters following the inhibition reaction.

The chemical structures of piperic acid and its lipophilic ester derivatives are shown in Figure 1.

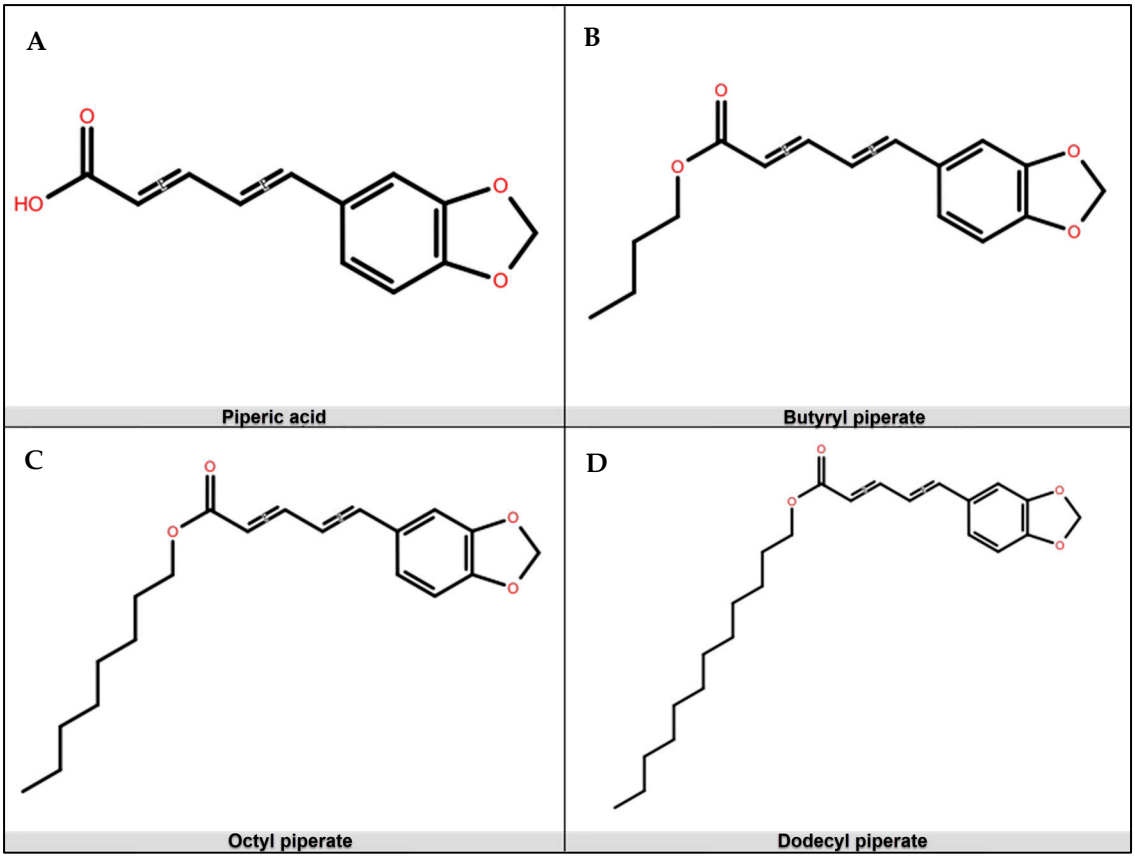


Figure 1. Two-dimensional chemical structures of piperic acid and its enzymatically synthesized lipophilic ester derivatives. (**A**) Piperic acid (PA); (**B**) Butyryl piperate (C4, R1); (**C**) Octyl piperate (C8, R2); (**D**) Dodecyl piperate (C12, R3).

2.2. Enzyme

Rhizopus oryzae was isolated from rotten olives in our laboratory. *Rhizopus oryzae* lipase (ROL) was produced and purified to homogeneity as described previously [19].

2.3. Lipase Activity Measurement

Lipase hydrolytic activity was measured using a pH–Stat (Metrohm AG, Herisau, Switzerland) with a 10% olive oil emulsion under the optimal conditions described previously [19]. One unit (IU) of lipase activity corresponds to the amount of enzyme that liberates 1 µmol of fatty acid per minute at pH 8.5 and 37 °C.

2.4. Lipase Inhibition Measurement

The inhibitory effects of piperic acid derivatives on ROL were evaluated using three established protocols (Methods A, B, and C) [4,6]. Inhibitor concentrations ranging from 0.02 to 2.5 mg/mL were tested in triplicate.

Method A: In this assay, the lipase was pre-incubated with varying concentrations of piperic acid and its lipophilic derivatives (butyl, octyl, and dodecyl piperate) for 15 min at

room temperature in the absence of substrate. The residual lipase activity (%) was then measured using a 10% olive oil emulsion as substrate under standard conditions. Control activity (100%) was measured in the absence of inhibitors.

Method B: With this method, we studied the interaction between piperic acid and its esters with the enzyme during the hydrolysis of the olive oil emulsion. The inhibitors were added to the reaction mixture at different concentrations 2 min after enzyme addition. The inhibitory effect was determined by measuring lipolytic activity at pH 8.5 and 37 °C before and after the addition of the inhibitors.

Method C: In this case, different concentrations of inhibitors were pre-incubated with the substrate emulsion at pH 8.5 and 37 °C for 2 min before the addition of the *R. oryzae* lipase to the "poisoned substrate". The lipase activity was measured as above.

The percentage of inhibition was calculated using the following equation (Equation (1)):

$$\text{Inhibition (\%)} = (\text{T} - \text{E})/\text{T} \times 100 \quad (1)$$

where T and E are the lipase activities in the absence and the presence of inhibitors, respectively.

IC50 values were defined as the inhibitor concentrations that reduce the lipase activity by 50%. These concentrations were extracted from the experimental curves [4,12].

2.5. Molecular Docking Analysis

2.5.1. Protein Structure Preparation and Validation

To investigate the binding interactions between *Rhizopus oryzae* lipase and the piperic acid derivatives, molecular docking was conducted using the three-dimensional structure of (UniProt ID: P61872), retrieved from the AlphaFold Protein Structure Database (AF-P61872-F1) [33], comprising residues 1–392.

The structural integrity and stereochemical quality of the model were validated using multiple online servers, including MolProbity [24], PROCHECK [34], ProSA-web [35], ERRAT [36], and VERIFY3D [37]. Protein preparation was performed using the Protein Preparation Wizard (Schrödinger Suite) [38]. The process was conducted at a physiological pH of 7.4 to mimic in vivo conditions. This procedure involved assigning proper bond orders, adding hydrogens, optimizing the protonation states of ionizable residues, and refining the hydrogen-bonding network. Finally, the AlphaFold v2.0-predicted structure of *R. oryzae* lipase (AF-P61872-F1, residues 1–392), was subjected to restrained energy minimization using the OPLS4 force field through a 150 ns molecular dynamics simulation [22] with a heavy-atom convergence criterion of 0.30 Å RMSD. This step was crucial for refining the predicted structure and ensuring its stability and quality before proceeding with the docking analysis.

2.5.2. Ligand Preparation and Molecular Docking

Piperic acid and its derivatives (butyryl, octyl, and dodecyl piperate) were prepared using LigPrep v5.8 implemented in Schrödinger Suite 2023-4 (Schrödinger, LLC, New York, NY, USA) [38]. Ionization states were generated at a physiological pH of 7.4 ± 0.2. Relevant tautomers and low-energy stereoisomers were enumerated and minimized using the OPLS4 force field [39] to obtain a representative set of conformers for docking. Molecular docking was performed using the Glide v9.1 XP (extra precision) protocol (Schrödinger Suite 2023-4) [40]. Based on previous studies on lipase inhibition, a cubic bounding box (10 Å × 10 Å × 10 Å) was centered on the catalytic triad of the active site (Ser268, Asp327, His380) to enable accurate binding pose prediction [41]. Orlistat, a well-known covalent lipase inhibitor, was retained in the analysis as a relative scoring reference only. To account for receptor flexibility, Induced Fit Docking (IFD) [42] was applied. The protocol included

an initial Glide docking step with softened van der Waals potentials, refinement of receptor side chains within a 5 Å radius of the ligand using Prime v5.8 [43], and subsequent redocking into the newly relaxed binding site. Poses were scored using the XP scoring function, and the most favorable ones were selected for further analysis. Protein–ligand interactions were evaluated according to standard geometric criteria, including hydrogen bonds, hydrophobic interactions, and π–π stacking [44]. Precise distances between ligands and catalytic residues were also quantified for each top-ranked pose.

2.6. Molecular Dynamics (MD) Simulations

Molecular dynamics (MD) simulations were conducted using Desmond v5.3 (Schrödinger Suite) within the Maestro interface on a Fedora39 operating system equipped with an RTX 3050Ti GPU (6 GB VRAM). Simulations were performed for both the apo form of the lipase and its complexes with piperic acid derivatives and orlistat. Each system was solvated using the explicit TIP3P water model [45] within an orthorhombic box, ensuring a 10 Å buffer from the protein surface. Counter ions (Na^+, Cl^-) were added to neutralize the system and achieve a physiological ionic strength of 0.15 M. After steepest descent energy minimization (2500 steps) to remove steric clashes, systems underwent multi-step equilibration with positional restraints on heavy protein atoms. Production simulations were run for 150 ns under NPT conditions (300 K, 1 atm), employing the Nosé–Hoover thermostat [46] and the Martyna–Tobias–Klein barostat [47] for temperature and pressure control. Long-range electrostatics were computed using the Particle Mesh Ewald method [48] with a 9.0 Å cutoff for short-range interactions. Trajectories were recorded at 1-ns intervals and analyzed using Simulation Interaction Diagrams (SID) implemented in Desmond of Schrödinger Suite 2023-4 [38]. For each ligand–protein complex, the top-ranked Induced Fit Docking (IFD) pose was used as the starting structure for molecular dynamics simulations (Schrödinger Suite 2023-4), as IFD accounts for receptor flexibility and provides a physically realistic binding conformation.

2.7. Binding Free Energy Calculations

Binding free energies (ΔGbind) were estimated using the Molecular Mechanics/Generalized Born Surface Area (MM-GBSA) method implemented in Prime [42]. MM-GBSA calculations were performed using the Thermal Prime protocol. Snapshots were extracted every 10 frames (1 ns) starting from frame 500 (50 ns), after discarding equilibration, yielding 100 snapshots per complex over the 50–150 ns production window, as determined by RMSD stability. The ΔGbind values were decomposed into van der Waals, electrostatic, polar solvation (using the VSGB 2.0 model), non-polar solvation, and ligand strain components [49]. Per-residue energy decomposition was also performed to identify the key residues contributing most favorably to ligand binding. All ΔGbind values are reported as mean ± standard error of the mean (SEM), calculated as $SD/\sqrt{n}$, where n = 100 snapshots.

3. Results

3.1. Inhibitory Effect of Piperic Acid and Its Lipophilic Derivatives on R. oryzae Lipase

This study assessed the inhibitory effects of newly synthesized lipophilic piperate esters [17] on *R. oryzae* lipase (ROL) using three inhibition methods.

Method A: Pre-incubation in an aqueous medium was performed without substrate to evaluate direct interactions between ROL and piperic acid or its derivatives. The inhibitory effects at different concentrations are presented in Figure 2A. At 2.5 mg/mL, butyl piperate inhibited 91% of ROL activity, while almost 80% inhibition was obtained with piperic acid, octyl piperate, and dodecyl piperate. Notably, octyl piperate showed the lowest IC_{50} (0.25 mg/mL), followed by piperic acid (0.4 mg/mL), whereas dodecyl piperate was the

least potent (IC_{50} = 0.9 mg/mL). These findings indicate that lipophilization of piperic acid with an octyl chain enhances ROL inhibition. Many studies have reported that hydrophobic natural compounds can act as potent inhibitors for pancreatic and bacterial lipases [4,50].

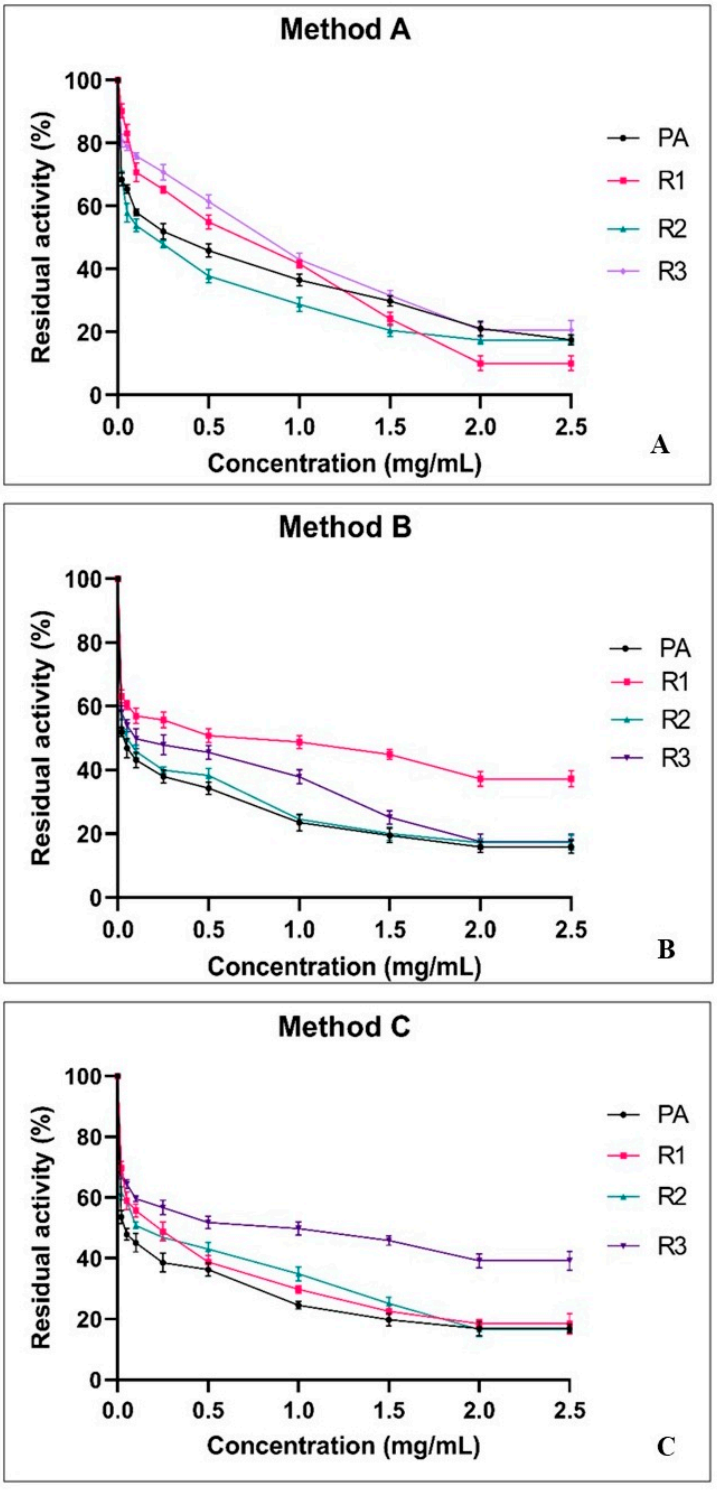


Figure 2. Effect of piperic acid (PA), butyryl piperate (R1), octyl piperate (R2), and dodecyl piperate (R3) on *Rhizopus oryzae* lipase (ROL) activity. (**A**) Inhibition using Method A. The ROL was pre-incubated at 25 °C for 10 min with different concentrations of the piperic acid and its derivatives. (**B**) Inhibition using Method B. The piperic acid and its lipophilic derivatives were added during olive oil emulsion hydrolysis at pH 8.5 and 37 °C. (**C**) Inhibition using Method C. The piperic acid and its esters were added to an olive oil emulsion at pH 8.5 and 37 °C before lipase injection. All the obtained results are expressed as the means of three experiments ± standard deviation.

Method B: This method was employed to determine the enzyme inhibition during hydrolysis. Various concentrations of piperic acid or its derivatives were added 2 min after ROL addition to the olive oil emulsion at pH 8.5 and 37 °C. Our results (Figure 2B) show 62% inhibition of ROL activity at 2.5 mg/mL butyl acetate, while, at the same concentration, piperic acid and its octyl and dodecyl esters achieved 84% inhibition. Both piperic acid and octyl piperate exhibited the most remarkable inhibitory effects with IC50 values of approximately 0.05 mg/mL. This observed inhibitory effect may result from a direct action on the adsorbed enzyme and/or an alteration of the lipid-water interface, which affects the enzyme binding step.

Method C: The inhibition of ROL by the "poisoned substrate" method was performed with different concentrations of the piperic acid and its lipophilic derivatives. In this case, inhibitors were pre-incubated with the substrate for 2 min before enzyme addition. The results are presented in Figure 2C. This figure shows 60% inhibition of ROL activity by 2.5 mg/mL dodecyl acetate with an IC50 of 0.8 mg/mL. However, a comparable ROL inhibitory effect of 80% was observed with 2.5 mg/mL piperic acid or its butyl- and octyl esters (Figure 2C). Piperic acid and octyl piperate again showed the most potent inhibitory effects, with IC_{50} values of approximately 0.05 mg/mL and 0.15 mg/mL, respectively.

Overall, the physicochemical properties of the inhibitors strongly influence ROL inhibition in Method C, likely due to their ability to bind at the lipid–water interface and modify interfacial properties that govern enzyme activity. The possibility that piperate esters act as competing substrates rather than true inhibitors was considered by HPLC analysis. Our results show that no detectable hydrolysis products were observed over the timescale of the inhibition assay (Figure S1).

3.2. In Silico Structural Analysis

3.2.1. Structural Validation of AlphaFold Model

The AlphaFold-predicted structure of *Rhizopus oryzae* lipase (ROL) was validated using multiple structural assessment tools to confirm its reliability for molecular docking and dynamics simulations. MolProbity analysis yielded a clashscore of 2.02 and a MolProbity score of 1.19, ranking the model in the 99th percentile relative to experimentally determined structures.

Ramachandran plot analysis revealed that 96.6% of residues fell within favoured regions, with no outliers (Figure 3).

Additional validation using PROCHECK showed that 86.0% of residues were in core regions, 12.2% in allowed regions, and 1.1% in disallowed regions. The ProSA Z-score (−8.33) fell within the range of native protein structures of comparable size.

VERIFY3D analysis revealed that 84.3% of residues had acceptable 3D/1D compatibility scores, while ERRAT yielded an overall quality factor of 89, exceeding the threshold of 80 established as indicative of a high-quality structural model [36].

Minor structural deviations were observed, including three cis-Proline residues, 0.7% poor rotamers, 1.0% bond angle outliers, and 1.6% CaBLAM outliers. Such deviations are typical in predicted models, particularly within flexible loop regions [51,52], and do not compromise the overall structural quality.

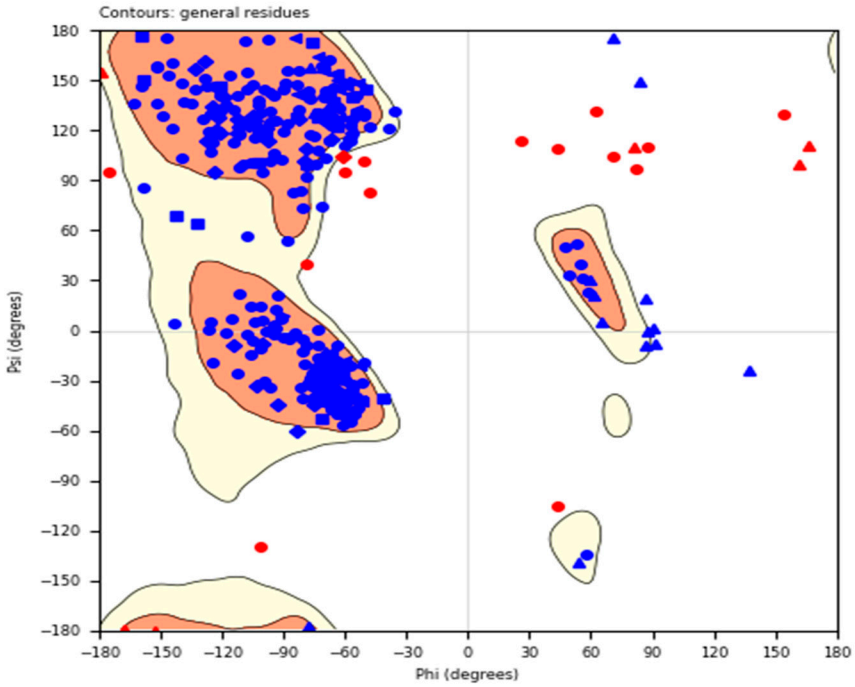


Figure 3. Ramachandran plot of the structural model of *Rhizopus oryzae* lipase. Red, yellow, and light-yellow regions represent most favored, allowed, and generously allowed conformations, respectively. White areas correspond to disallowed regions. Blue triangles and circles represent non-glycine and non-proline residues, respectively. Red points indicate outlier residues.

3.2.2. Molecular Docking Analysis

To gain structural insights into the anti-lipase activity of piperic acid and its various derivatives, we employed molecular docking to examine their binding affinities and interaction profiles with key amino acids in the active site of *R. oryzae* lipase. Docking simulations were performed using two approaches within the Schrödinger software suite: Glide XP (extra precision) and Induced Fit Docking (IFD).

Since no experimental structure of ROL or any Rhizopus lipase complexed with a non-covalent inhibitor is available in the RCSB Protein Data Bank, formal redocking validation was not feasible. Instead, protocol reliability was evaluated through concordance among Glide XP scores, MM-GBSA binding free energies, 150 ns MD stability profiles, and experimental IC_{50} values.

The results from these studies allowed us to establish structure-function relationships, shedding light on the potential lipolysis-inhibitory properties of the piperic acid derivatives. An overview of the structural model of the *R. oryzae* lipase/piperate ester complex is presented in Figure 4. Docking scores and binding affinities are summarized in Table 1.

Table 1. Docking Parameters for Piperic Acid Derivatives and Reference Inhibitor.

Compound	XP Gscore (kcal/mol)	IFD Score
Octyl piperate	−11.134	−793.08
Orlistat (reference) †	−10.546	−795.41
Piperic acid	−9.912	−715.50
Butyryl piperate	−9.243	−790.55
Dodecyl piperate	−8.462	−791.10

† Orlistat is a covalent serine lipase inhibitor. The reported XP Gscore reflects non-covalent interactions only and does not represent its actual binding mechanism or inhibitory potency. Included for relative scoring context only.

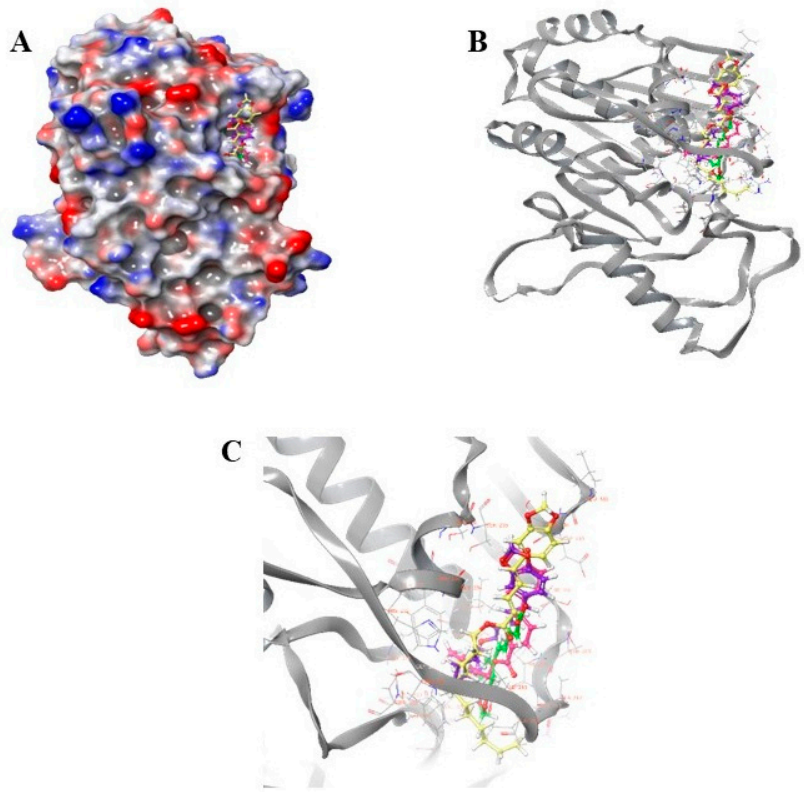


Figure 4. Structural model of the *R. oryzae* lipase/piperate ester complex with a GRASP (**A**) and ribbon (**B**) representation. (**C**) Zoom in on the interaction site between the enzyme and the different molecules.

This table presents the docking parameters obtained from Glide XP and Induced Fit Docking (IFD) approaches for piperic acid and its derivatives, alongside the reference Inhibitor. Among the compounds studied, octyl piperate emerged as the most potent inhibitor with a superior XP Gscore (−11.134 kcal/mol) compared to orlistat (−10.546 kcal/mol), representing a 5.6% improvement in rigid docking affinity. While orlistat showed marginally better IFD performance (−795.41 vs. −793.08), the minimal difference (0.3%) indicates comparable binding when accounting for protein flexibility. This dual-protocol analysis confirms octyl piperate's exceptional binding potential, with the eight-carbon alkyl chain achieving optimal hydrophobic complementarity within the enzyme's active site. The compound established a comprehensive interaction network including: (i) extensive hydrophobic contacts with Ala212, Pro301, Val329, Ile216 forming the primary binding core, (ii) π-alkyl interactions with Phe209 and His232 providing aromatic stabilization, and (iii) strategic positioning allowing multiple van der Waals contacts that maximize binding surface area while minimizing steric clashes (Figure 5A,B). These findings are consistent with the in vitro results, including a strong affinity between octyl piperate and the active site of *R. oryzae* lipase. The anti-lipase activity of octyl piperate showed high IC50 values (0.05 mg/mL with Methods B and C, and 0.25 mg/mL with Method A). This suggests that octyl piperate is a promising candidate for inhibiting the activity of this fungal enzyme. Orlistat was included as a relative scoring reference only. As a covalent serine lipase inhibitor that irreversibly acylates Ser268, its XP Gscore (−10.546 kcal/mol) and IFD score (−795.41 kcal/mol) reflect non-covalent interactions only and do not represent its true binding mechanism or affinity. These values are therefore not directly comparable to those of the piperate derivatives and are provided for contextual reference only.

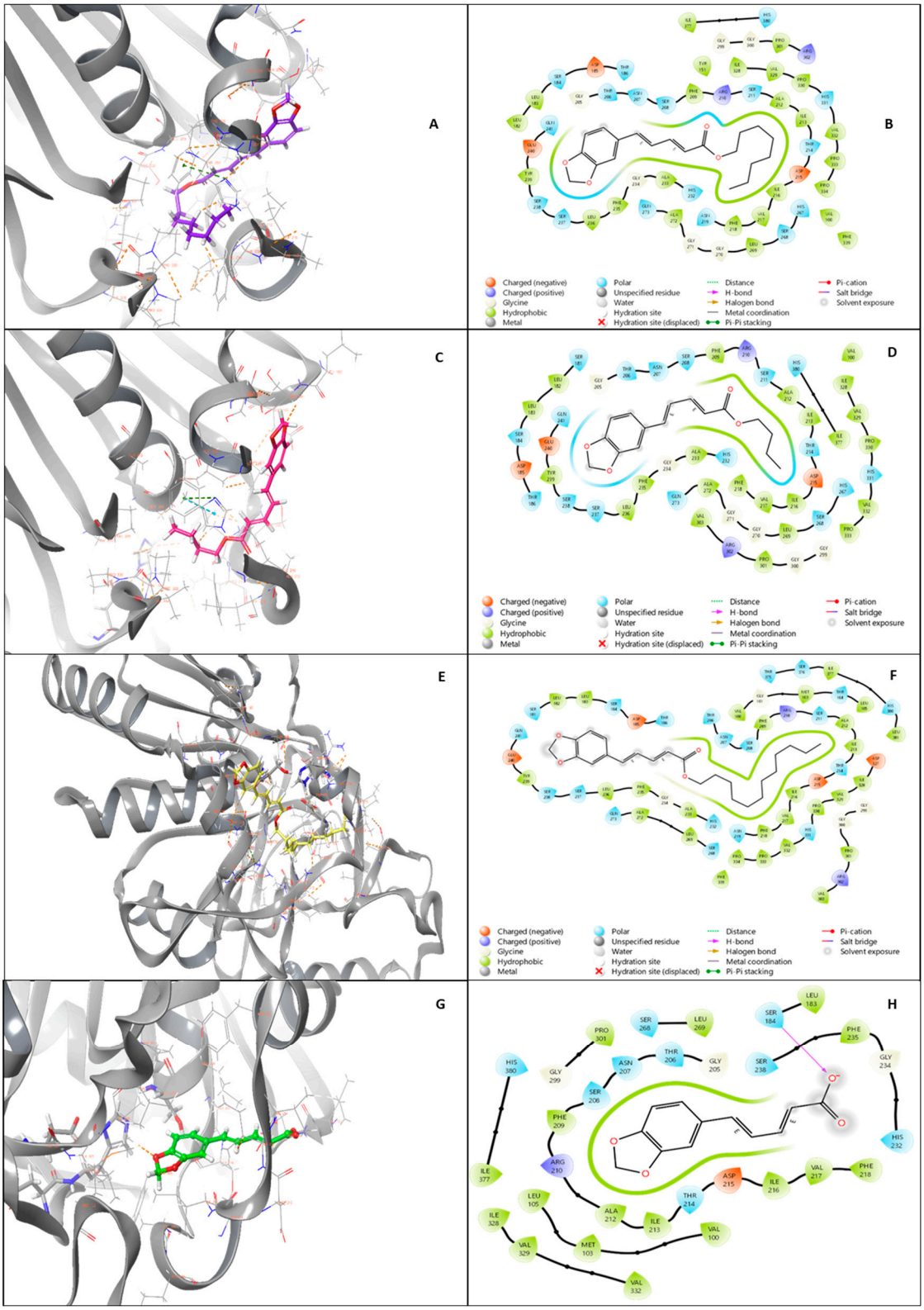


Figure 5. 3-D (left panel) and 2-D (right panel) representations of the binding site of piperic acid and its derivatives with *Rhizopus oryzae* lipase. (**A**,**B**) Octyl piperate/lipase complex; (**C**,**D**) Butyryl piperate/lipase complex; (**E**,**F**) Dodecyl piperate/lipase complex; (**G**,**H**) Piperic acid/lipase complex.

In contrast, butyryl piperate demonstrated moderate binding potential (XP: −9.243 kcal/mol; IFD: −790.55 kcal/mol) with a compensatory binding strategy. The shorter four-carbon chain limitation was offset by an enhanced hydrogen bonding capacity,

which formed stable H-bonds with Ser184 (active site proximity), Ile213 (backbone interaction), and Ser238 (side-chain hydroxyl group). Additional stabilization derived from hydrophobic interactions with Tyr151 and Leu269, creating a balanced binding mode that maintained reasonable affinity despite suboptimal chain length for the binding pocket dimensions (Figure 5D).

Dodecyl piperate, despite possessing the longest alkyl chain (12 carbons), showed an unexpectedly lower binding affinity (XP: −8.462 kcal/mol; IFD: −791.10 kcal/mol), as presented in Table 1, illustrating the principle that excessive hydrophobic extension can be counterproductive. The extended chain formed multiple hydrophobic contacts with Pro301, Val329, Val332, Ile216, Leu105, Ile328, and Ile377, but likely encountered steric hindrance and unfavorable conformational constraints within the binding cavity (Figure 5E,F). The significant difference between XP and IFD scores suggests that protein flexibility partially accommodates the extended chain, but entropic penalties and reduced binding complementarity ultimately limit overall affinity. This finding establishes an optimal alkyl chain length threshold and demonstrates that binding affinity follows a bell-shaped relationship with hydrophobic chain extension in this system.

Finally, we examined the docking of the precursor compound, piperic acid, within the active site of the fungal lipase. As shown in Table 1, piperic acid exhibited moderate binding affinity (XP: −9.912 kcal/mol; IFD: −715.50 kcal/mol) through a distinct interaction mechanism. The compound primarily relied on hydrogen bonding networks with Thr206, Val217, His232, and the catalytic Ser268, supplemented by π-π stacking interactions with Phe209 and hydrophobic contacts with Gly205 and Val329 (Figure 5G,H). Despite forming stable electrostatic interactions, the lack of extended hydrophobic regions limited its overall binding affinity compared to the ester derivatives, highlighting the critical role of lipophilic modifications in enhancing lipase binding.

The docking protocol's reliability is supported by concordance among Glide XP scores, MM-GBSA binding energies, and MD simulation stability, all identifying octyl piperate as the most potent and dodecyl piperate as the weakest inhibitor, consistent with experimental IC_{50} values. Minor discrepancies, such as similar IC_{50} values for piperic acid and octyl piperate under Method B despite different XP Gscores, reflect known limitations of scoring functions for interfacial enzymes and do not affect the main conclusions. Overall, molecular docking of piperic acid derivatives corroborated in vitro results, highlighting octyl piperate as the most effective inhibitor. These findings emphasize the role of alkyl chain length in optimizing binding affinity and specificity, providing a foundation for the rational design of potent lipase inhibitors for industrial and therapeutic applications.

3.3. Molecular Dynamics Simulation Analysis (MD)

3.3.1. Root-Mean-Square Deviation (RMSD)

Root-Mean-Square Deviation (RMSD) measures the average distance between atoms, typically backbone atoms, of superimposed proteins and/or ligands [53]. In our molecular dynamics simulations, the RMSD was used to reveal the structural stability of the ROL complexed with each of the piperic acid and its derivatives. This study conducted a 150-nanosecond MD simulation to monitor the dynamic behavior of each enzyme-ligand complex over time (Figures S2–S6).

The comprehensive 150 ns molecular dynamics simulations revealed distinct conformational stability profiles for each lipase-ligand complex, with all systems achieving equilibration within 20–30 ns but exhibiting characteristic ligand-specific behaviors thereafter. Protein backbone stability was excellent across all complexes, with RMSD values ranging from 2.0 to 2.8 Å, well within the acceptable limits for globular proteins. The apo lipase reference showed slightly higher fluctuations (2.5–3.2 Å), confirming that ligand bind-

ing provides overall stabilization to the enzyme structure. The catalytic domain (residues 200–380) demonstrated exceptional stability across all complexes (RMSD < 2.0 Å), while N-terminal regions (residues 1–50) exhibited moderate flexibility (2.5–3.5 Å) consistent with surface loop dynamics.

The five compounds exhibited markedly different ligand mobility patterns, which directly correlated with their binding mechanisms and structural features. Orlistat demonstrated exceptional binding stability, characterized by a two-phase profile, with rapid equilibration within the first 10 ns and subsequent stabilization at approximately 2.5 ± 0.3 Å for the remainder of the simulation. Initial optimization (0–25 ns) exhibited moderate fluctuations (ligand RMSD, 2.0–3.8 Å) as the complex pharmacophore groups optimized their positions, followed by remarkable stability (RMSD, 2.1 ± 0.3 Å, for 25–150 ns), reflecting the compound's optimized design for lipase binding. This stability profile validates orlistat's clinical efficacy and provides a benchmark for evaluating novel inhibitors of this class.

The profiles shown in Figure 6A suggest that the formation of the lipase/butyryl piperate complex stabilizes over the course of the 150 ns simulation. Butyryl piperate demonstrated intermediate stability with ligand RMSD fluctuating between 1.2–2.0 Å, while protein backbone RMSD values stabilized within the first 20 ns and remained consistently below 2.5 Å. The four-carbon chain exhibited restricted mobility due to its optimal fit within a hydrophobic sub-pocket, while the piperate head group maintained consistent hydrogen bonding geometry. Occasional RMSD spikes reaching 2.5 Å at 45 ns and 110 ns corresponded to transient chain rotations around the ester linkage, indicating modest conformational flexibility without loss of binding affinity. The ligand maintained a stable binding pose within the active site, with fluctuations remaining below 1.5 Å throughout the trajectory.

In contrast, the RMSD of the octyl piperate (Figure 6B) revealed a biphasic stability profile with distinct conformational phases, as the protein backbone RMSD exhibited initial equilibration within the first 20 ns, followed by stabilization at around 2.8 ± 0.4 Å. Notably, Initial equilibration (0–30 ns) showed high ligand mobility (RMSD 2.0–4.5 Å) as the eight-carbon chain explored multiple orientations within the binding pocket. A significant conformational transition occurred around 40–50 ns (RMSD peak at 4.2 Å), followed by stabilization into a preferred binding mode after 70 ns (RMSD 2.5 ± 0.4 Å). This behavior suggests an induced-fit mechanism, where both the ligand (octyl piperate) and the protein (*R. oryzae* lipase) undergo mutual adaptation to achieve optimal complementarity, with the stabilized conformation persisting for the final 80 ns, indicating a thermodynamically favorable binding.

Figure 6B also shows that the overall RMSDs for the protein and ligand reached a relatively steady state between 80 and 100 ns. This indicates that the simulations had likely converged and that the system had adequately explored a representative range of conformations.

Dodecyl piperate (Figure 6C) exhibited the highest conformational flexibility, with ligand RMSD ranging from 1.5 to 6.5 Å and multiple distinct binding phases, while the protein backbone RMSD stabilized around 2.5–3.0 Å after initial equilibration. The extended 12-carbon chain showed continuous conformational sampling, with major transitions at 40 ns (RMSD jump to 5.8 Å) and 65 ns (stabilization at 4.2 Å). Analysis of chain end-to-end distances revealed the alkyl tail exploring regions both within and extending beyond the primary binding pocket, suggesting partial solvent exposure. Despite high mobility, the piperate head group maintained consistent interactions with the active site, indicating a "molecular anchor" binding mode where the pharmacophore remains fixed while the extended chain samples multiple conformations (Figure 6C).

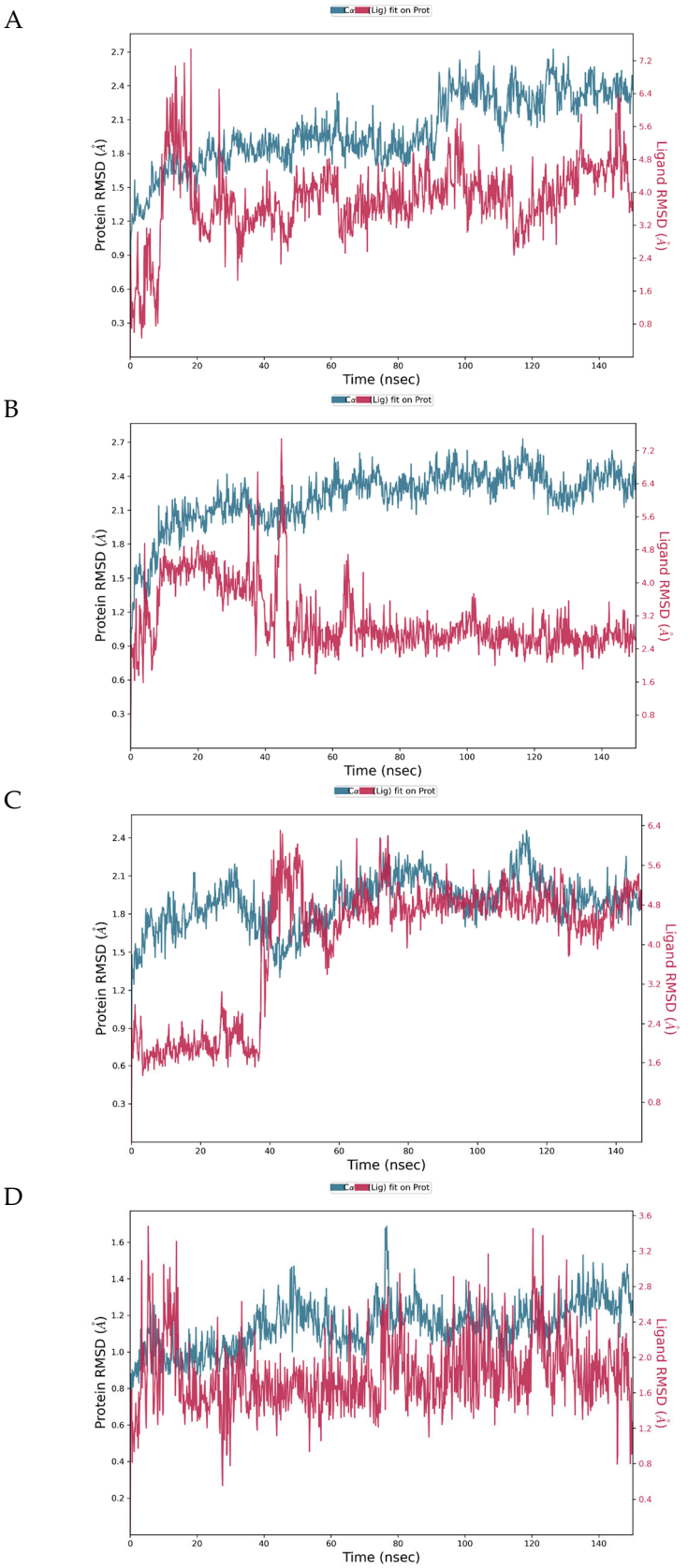


Figure 6. The root means square deviation (RMSD) of (**A**) Butyryl piperate/lipase complex; (**B**) Octyl piperate/lipase complex; (**C**) Dodecyl piperate/lipase complex; (**D**) Piperic acid/lipase complex. The blue color indicates fluctuations in the enzymatic protein. The RMSD of the ligand is indicated in red.

Piperic acid exhibited the most rigid binding behavior with ligand RMSD consistently below 1.8 Å throughout the entire trajectory (Figure 6D). The compound achieved rapid equilibration within 10 ns and maintained a single, well-defined binding conformation, reflecting strong electrostatic anchoring through hydrogen bonds with the catalytic serine and surrounding polar residues. The minimal conformational sampling suggests high binding site complementarity despite the absence of extended hydrophobic interactions. The protein backbone RMSD fluctuated within an acceptable range of 1.0–2.5 Å relative to the initial conformation, indicating minimal large-scale conformational changes (Figure 6D). These findings suggest that the lipase/piperic acid complex attained a stable conformation following the initial adjustment phase.

3.3.2. Root-Mean-Square Fluctuation (RMSF)

RMSF values for the backbone atoms of the protein and ligand were calculated as a function of simulation time to assess residue-level flexibility (Figures S2–S6). In molecular dynamics simulations, average RMSF values are commonly used as an indicator of the overall flexibility of a system [54]. The RMSFs of each backbone atom were calculated for every residue to identify regions of structural fluctuation.

Per-residue flexibility analysis revealed ligand-specific effects on protein dynamics and identified critical binding regions through perturbations in mobility. All complexes maintained characteristic protein flexibility signatures with terminal regions (residues 1–25 and 370–392) showing the highest fluctuations (RMSF > 3.0 Å), intermediate flexibility in surface loops (RMSF 1.5–2.5 Å), and rigid core secondary structures (RMSF < 1.5 Å). The catalytic triad (Ser268, Asp327, His380) consistently exhibited minimal fluctuations (RMSF < 0.8 Å), confirming structural integrity essential for catalytic function. Comparative analysis with apo lipase revealed significant stabilization of the binding site across all complexes, with the primary binding pocket (residues 200–220, 265–280, 325–340) exhibiting a 25–40% reduction in RMSF values upon ligand binding. Octyl piperate provided the most pronounced stabilization (38% average RMSF reduction in binding residues), while piperic acid showed the least effect (22% reduction), correlating with their respective binding affinities.

Secondary structure analysis throughout the MD trajectories confirmed robust structural integrity across all complexes. All systems maintained a helical content of 24.96–26.06%, compared to 25.8% in crystal structures, with octyl piperate showing the highest conservation (26.06%) and dodecyl piperate exhibiting the most variation (24.96%). β-sheet content remained stable at 18.45–20.51% across all complexes, with the central β-sheet core showing exceptional conservation. Ligand binding enhanced β-sheet stability, particularly in the substrate-binding region, supporting the role of induced-fit stabilization. The total secondary structure element content ranged from 43.71% (piperic acid) to 46.42% (octyl piperate), indicating excellent structural preservation throughout the simulations.

Protein-ligand interaction analysis revealed distinct interaction profiles for each compound. Orlistat established exceptional binding stability with central pharmacophore regions showing minimal fluctuations (RMSF < 2.0 Å) and terminal aliphatic chains exhibiting moderate flexibility (RMSF 2.0–3.5 Å). The hydrogen bonding network showed exceptional stability with key interactions maintained at high occupancy rates exceeding 70% of simulation time, while extensive hydrophobic contacts demonstrated high temporal stability (>80% occupancy). Ionic interactions contributed significantly to binding stability with sustained electrostatic contacts throughout the trajectory.

Figure 7A shows that Butyryl piperate exhibited a diverse network of interactions contributing to stable binding, with hydrophobic contacts maintaining high occupancy throughout the simulation (>70% of trajectory time) and hydrogen bonding interactions showing moderate but consistent occupancy (40–60%). Water-mediated interactions were

observed sporadically (15–25%), while ionic interactions were minimal, reflecting the neutral charge state and predominantly hydrophobic character of the binding site. The overall protein flexibility was well-maintained, with the catalytic triad region showing minimal fluctuations (RMSF < 1.0 Å), indicating that butyryl piperate did not disrupt the essential catalytic architecture.

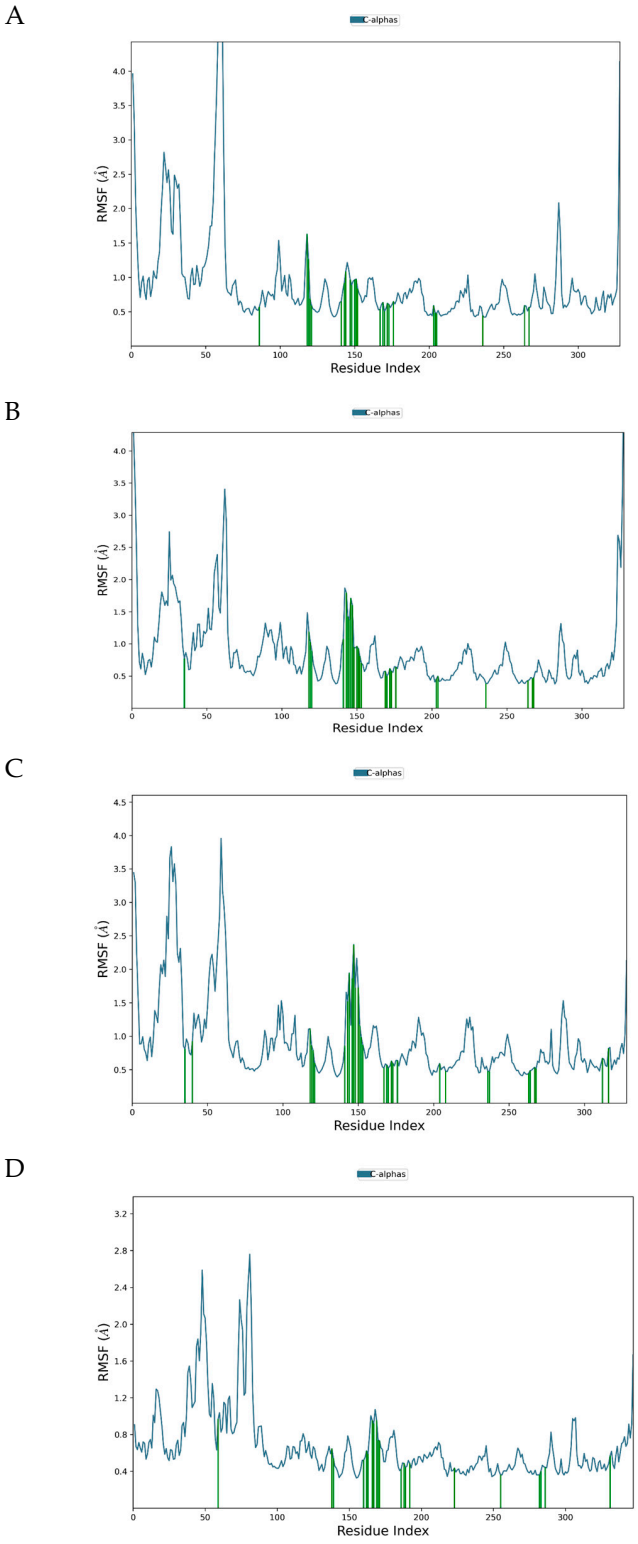


Figure 7. Root-Mean-Square Fluctuation (RMSF) of (**A**) Butyryl piperate/lipase complex; (**B**) Octyl piperate/lipase complex; (**C**) Dodecyl piperate/lipase complex; (**D**) Piperic acid/lipase complex. The green-colored vertical bars correspond to the enzyme residues that interact with the ester.

The RMSF profile (Figure 7B) revealed distinct patterns of residue fluctuations in the Lipase/Octyl piperate complex during the 150 ns MD simulations. Octyl piperate demonstrated binding primarily driven by hydrophobic interactions, which dominated the binding interface with total contact occupancy fluctuating between 6 and 12 interactions per frame. Hydrogen bonding interactions showed relatively low occupancy (<30% simulation time), suggesting that binding is primarily driven by hydrophobic and van der Waals forces rather than specific polar contacts. Water-mediated interactions contributed through several transient water bridges between ligand and protein residues. The ligand containing 11 rotatable bonds exhibited considerable conformational flexibility, with the octyl chain terminus displaying the highest atomic fluctuations (>2.5 Å) while the piperonyl moiety remained more constrained within the binding site.

RMSF analysis identified protein regions with high RMSF values (greater than 3 Å), indicating significant flexibility (Figure 7C). This inherent mobility is hypothesized to be crucial in accommodating the bound ligand. Such flexibility may enable localized conformational adjustments around the bound ligand, facilitating the exploration of various binding conformations and contributing to optimal ligand positioning. Alternatively, the presence of the ligand could induce conformational changes in these dynamic regions, suggesting a mechanism of induced fit that stabilizes the final complex structure.

Dodecyl piperate established multiple intermolecular contacts throughout the trajectory, with key hydrogen bonds showing occupancy values ranging from 15% to 65% of simulation time. The extended dodecyl chain established extensive hydrophobic contacts with high occupancy rates (>70% for several residues), while water bridge formation was observed between ligand and protein, particularly involving polar regions. The total number of protein-ligand contacts fluctuated between 8 and 15 interactions per frame, indicating a stable yet flexible binding mode. The molecule's 15 rotatable bonds allowed substantial conformational sampling, with the dodecyl chain adopting multiple conformational states while maintaining overall molecular compactness.

The RMSF profile (Figure 7D) revealed increased flexibility in the N-terminal side of the fungal lipase. Interestingly, the residues involved in interactions with the piperic acid ligand showed reduced fluctuations, which could contribute to stabilizing the enzyme-ligand complex.

Piperic acid demonstrated a comprehensive interaction network comprising hydrogen bonds, hydrophobic interactions, ionic interactions, and water-mediated bridges. Hydrogen bonds constituted the primary stabilizing interactions, with an average of 2–3 simultaneous H-bonds maintained throughout the simulation and occupancies ranging from 15% to 85%. The aromatic ring system engaged in significant hydrophobic contacts and π-π stacking interactions, with occupancies of 30–70%. Meanwhile, the negatively charged carboxylate group formed ionic interactions with positively charged residues, exhibiting occupancies of 20–60%.

Ligand conformational analysis revealed distinct flexibility patterns correlating with chain length and binding mechanisms. Piperic acid showed moderate flexibility in its three rotatable bonds, with the carboxylate group and conjugated chain system exhibiting different degrees of flexibility while maintaining a constant radius of gyration (~4.2 Å). Butyryl piperate's seven rotatable bonds exhibited varying degrees of flexibility, with the aliphatic chain region displaying the highest conformational freedom. Probability density distributions indicated stable conformational states without significant energy barriers. Octyl and dodecyl piperates demonstrated increasing conformational complexity due to their extended alkyl chains, which allowed for multiple orientations while maintaining core pharmacophore interactions with the active site.

Based on combined RMSD, RMSF, and secondary structure metrics, the complexes ranked in stability as orlistat > piperic acid > butyryl piperate > octyl piperate > dodecyl piperate. Notably, this ranking differs from binding affinity, highlighting that conformational stability and binding strength can be independent properties in structure-based drug design. The molecular dynamics simulations provide comprehensive insights into the dynamic behavior of piperic acid derivatives in complex with *Rhizopus oryzae* lipase, revealing distinct binding mechanisms and conformational preferences that correlate with their inhibitory potentials and establishing a foundation for rational optimization of piperate-based lipase inhibitors.

3.3.3. Analysis of Interactions Involved in the Formation of the Lipase-Ligand Complex

Analysis of the average interaction frequencies (Figures S2–S6) suggests that a network of key residues is crucial in stabilizing the lipase/butyryl piperate complex. Notably, Tyr151 (via its hydroxyl group), Leu183 (through aliphatic side chain carbons), and Ser184 (hydroxylated residue) form hydrogen bonds and hydrophobic contacts with the ligand (Figure 8A,B). Although the ligand displays conformational flexibility during the simulation, as indicated by the torsional angle variations in the RMSF profile (Figure 8A). It eventually adopts a relatively stable conformation within the lipase-binding pocket, suggesting a favorable binding mode. Additional interactions, including a hydrogen bond with His232 and hydrophobic interactions with Leu269 and Ile213, could further contribute to the stability of the complex.

In the lipase/octyl piperate complex, MD simulations reveal the dominant role of hydrophobic interactions in ligand binding. Octyl piperate, with its extended aliphatic chain, forms favorable van der Waals interactions with key residues such as Val332, Val329, and Ala212 (Figure 8C,D). These interactions create a hydrophobic environment within the binding pocket, facilitating a precise fit of the non-polar portion of the ligand. This hydrophobic complementarity is a fundamental principle in protein-ligand interactions, significantly contributing to the overall binding affinity of the complex. Beyond simple spatial proximity, the analysis suggests the possibility of aromatic stacking interactions between the ligand and phenylalanine residues (Phe209, Phe218, and Phe235) in the binding pocket. This π-π stacking stabilizes the complex and may influence the ligand's specific orientation. In addition, the presence of a positively charged benzene ring on the ligand implies the potential for a π-cation interaction with Leu269, adding another layer of complexity to the aromatic interactions involved in ligand recognition.

Although the current visualization highlights water-mediated interactions, the presence of hydrogen bond donors and acceptors on both the ligand and the surrounding lipase residues (Ser268, Thr206, and Gln241) suggests the existence of a complex hydrogen-bonding network. This network could be crucial in anchoring the ligand and facilitating its optimal orientation within the binding pocket (Figure 8D).

Analysis of the *R. oryzae* lipase/dodecyl piperate complex revealed key stabilizing forces that anchor the ligand within the enzyme's binding pocket. Residues such as Val195, Gly253, and His257 exhibited high interaction frequencies, underscoring their pivotal role in ligand binding. The multifaceted nature of the interaction is evident through a combination of hydrogen bonds, hydrophobic interactions, and residue-specific interactions. As illustrated in Figure 8E,F, crucial stabilizing forces include hydrophobic interactions between aliphatic residues (e.g., Ile213, Ile327) and the ligand's long aliphatic chain, potential π-π interactions of residues such as Phe 209 and Phe238, and hydrogen bonds involving His232, Ser237, and Thr206. This intricate network of interactions highlights the synergistic contribution of multiple forces in stabilizing the lipase-dodecyl piperate complex.

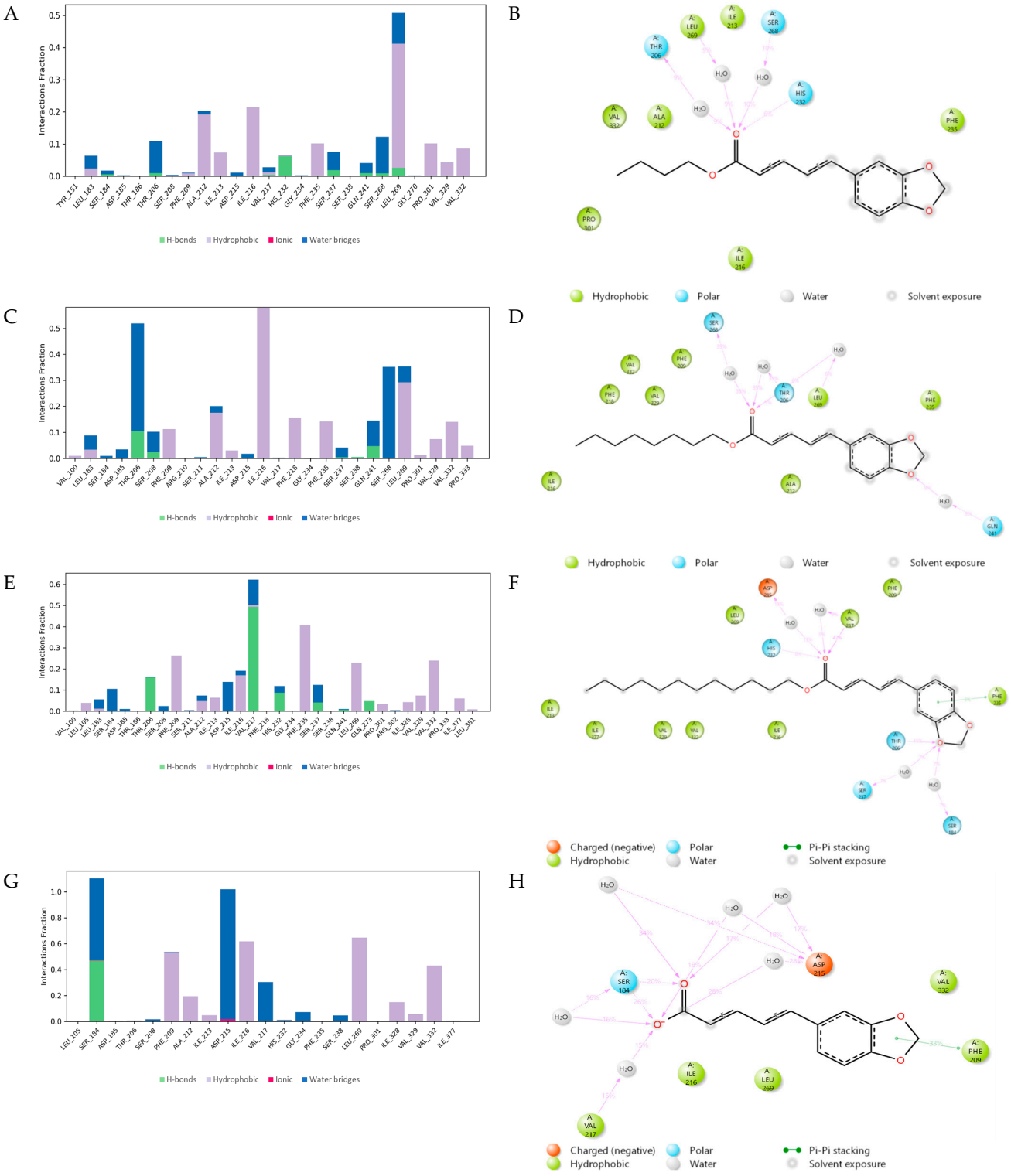


Figure 8. Interaction's frequencies (left panel) and amino acids residues (right panel) involved in the formation of (**A**,**B**) Butyryl piperate/lipase complex; (**C**,**D**) Octyl piperate/lipase complex; (**E**,**F**) Dodecyl piperate/lipase complex; (**G**,**H**) Piperic acid/lipase complex.

Finally, a detailed analysis of the interactions between *R. oryzae* lipase and piperic acid revealed a network of interactions crucial to the stability of the complex (Figure 8G,H). Key stabilizing interactions include hydrogen bonds involving Ser209, Val216, and Ile217, which possess functional side chains such as hydroxyl or amine groups. In addition, the model suggests the presence of a π-π stacking interaction with Phe209, along with potential

hydrophobic interactions involving Val216 and Ile217. Beyond these primary interactions, the analysis also indicates the possible involvement of ionic bonds with charged residues such as Lys, Arg, Asp, and Glu. These additional electrostatic interactions may further enhance the complex's binding affinity, specificity, and stability.

A molecular docking model was developed to gain deeper insight into the interactions between lipase and small fatty acid molecules [55]. In this study, the active site of CALB lipase comprises a catalytic triad (Ser 105, His 224, Asp 187) associated with a charge transfer mechanism. Gln 106 and Thr 40 also formed stable hydrogen bonds with negatively charged oxygen atoms.

Hydrogen bonding and hydrophobic interactions were identified as the primary mechanisms through which lipase binds to fatty acids. The results reveal that all tested fatty acids engage in hydrogen bonding interactions with key active site residues, particularly Ser 105. This can be attributed to the nucleophilic nature of Ser 105, which exhibits a strong affinity for water molecules in a biphasic system.

The docking binding energies were calculated in the following order of increasing magnitude: Ethyl valerate (−1.05 kcal/mol), ethyl hexanoate (−1.10 kcal/mol), ethyl heptanoate (−1.12 kcal/mol), ethyl octanoate (−1.12 kcal/mol), ethyl nonanoate (−1.17 kcal/mol), ethyl decanoate (−1.20 kcal/mol), ethyl laurate (−1.29 kcal/mol). These results indicate an increase in binding energy with the length of the fatty acid chain, suggesting an enhanced affinity between longer-chain fatty acids and CALB lipase. This trend supports the conclusion that the selectivity of the CALB active site increases with the carbon chain length of the fatty acid [56]. Interestingly, our study, compared to other previously reported lipase inhibitors [57–59], revealed that the enzymatically synthesized piperic acid esters, especially octyl piperate, can inhibit the fungal *R. oryzae* lipase by accommodating itself in the active-site binding pocket, driven by favorable hydrophobic interactions with residues Val329, Ala212, and Phe209, with a geometry that does not position the ester carbonyl for productive nucleophilic attack by Ser268, supporting an inhibitory mode of action.

3.3.4. Binding Energy Analysis and Quantitative Metrics

Binding free energy calculations were performed using the MM-GBSA (Molecular Mechanics Generalized Born Surface Area) method, with snapshots extracted every 1 ns from the equilibrated trajectory (50–150 ns), yielding 100 snapshots per complex. The binding energies revealed a clear ranking of inhibitory potential, which correlates well with both the docking results and experimental observations (Table 2).

Table 2. MM-GBSA Binding Energy Analysis.

Ligand	ΔG Bind (kcal/mol)	ΔG vdW (kcal/mol)	ΔG Coulomb (kcal/mol)	Ligand Strain (kcal/mol)
Octyl Piperate	−79.03 ± 4.67	−59.90	−5.52	3.24
Dodecyl Piperate	−68.26 ± 3.93	−52.47	−7.90	2.21
Orlistat	−55.44 ± 7.19	−47.62	−62.35	5.40
Butyryl Piperate	−51.69 ± 4.17	−40.16	−7.59	1.52
Piperic Acid	−44.13 ± 2.44	−36.09	6.97	0.75

The MM-GBSA results reveal distinct energetic profiles for each compound (Figure 9). Octyl piperate demonstrated the highest binding affinity (−79.03 kcal/mol), primarily driven by strong van der Waals interactions (−59.90 kcal/mol), which reflect optimal hydrophobic complementarity with the binding pocket. The moderate Coulombic contribution (−5.52 kcal/mol) and manageable ligand strain (3.24 kcal/mol) indicate favorable binding without a significant conformational penalty.

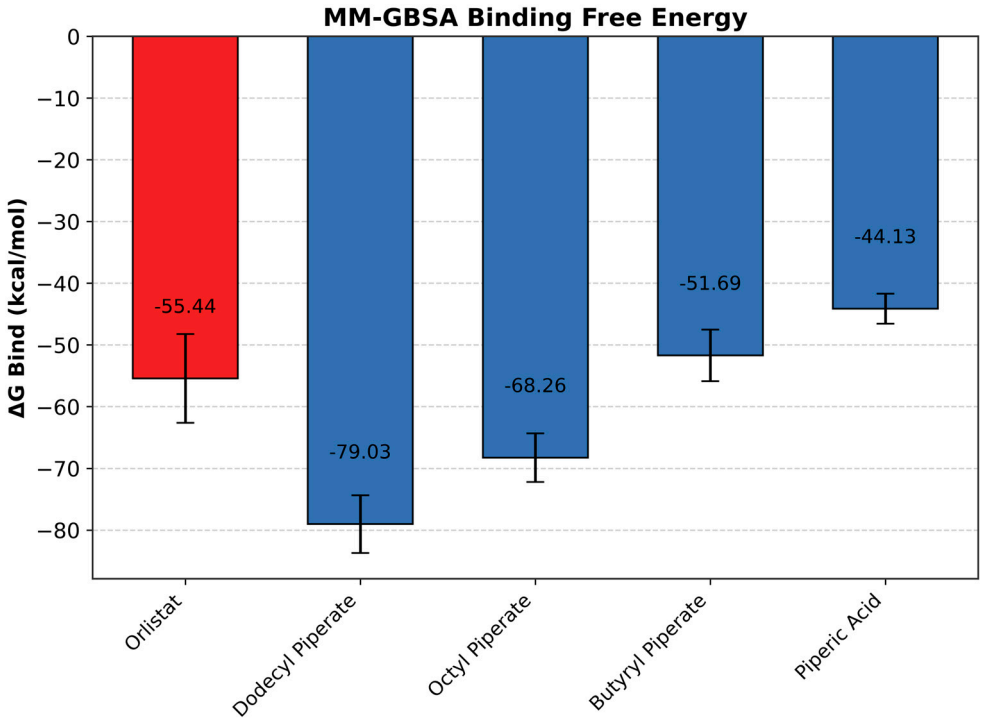


Figure 9. The results of MM-GBSA energetic profiles for the standard (red) and piperate esters (blue).

Dodecyl piperate exhibited the second-highest affinity (−68.26 kcal/mol), characterized by substantial van der Waals interactions (−52.47 kcal/mol) resulting from its extended alkyl chain. The enhanced Coulombic contribution (−7.90 kcal/mol) compared to shorter derivatives and low ligand strain (2.21 kcal/mol) suggests stable electrostatic interactions despite the molecule's flexibility.

Furthermore, Orlistat, despite being a known potent inhibitor, exhibited lower binding energy (−55.44 kcal/mol) in this analysis, though it uniquely showed the strongest Coulombic interactions (−62.35 kcal/mol), consistent with its polar functional groups and potential for covalent binding. The higher ligand strain (5.40 kcal/mol) may reflect conformational adjustments required for optimal active site complementarity.

In addition, Butyryl piperate demonstrated moderate binding (−51.69 kcal/mol) with balanced van der Waals (−40.16 kcal/mol) and Coulombic (−7.59 kcal/mol) contributions. The low ligand strain (1.52 kcal/mol) indicates minimal conformational stress upon binding.

Finally, Piperic acid showed the lowest binding affinity (−44.13 kcal/mol), with moderate van der Waals interactions (-36.09 kcal/mol) but a notably positive Coulombic energy (6.97 kcal/mol), suggesting that electrostatic repulsion partially offsets the hydrophobic binding. However, it exhibited the lowest ligand strain (0.75 kcal/mol), indicating optimal conformational compatibility with the binding site.

The energy decomposition reveals that van der Waals interactions dominate binding affinity across all piperate derivatives, with longer alkyl chains providing increasingly favorable hydrophobic contacts up to C8. The ranking Octyl > Dodecyl suggests an optimal chain length around C8, where hydrophobic binding is maximized without excessive entropic penalties or unfavorable conformational strain.

Interestingly, octyl piperate achieved significantly higher binding energy compared to the reference Orlistat, highlighting the effectiveness of hydrophobic optimization in this system and suggesting that the *R. oryzae* lipase active site is particularly suited for accommodating medium-chain fatty acid derivatives.

The comprehensive molecular dynamics analysis, supported by quantitative MM-GBSA binding energy calculations, revealed distinct binding profiles and established an apparent activity ranking: Octyl Piperate (−79.03 kcal/mol) > Dodecyl Piperate (−68.26 kcal/mol) > Orlistat (−55.44 kcal/mol) > Butyryl Piperate (−51.69 kcal/mol) > Piperic Acid (−44.13 kcal/mol).

Octyl piperate emerged as the most potent inhibitor, achieving 42% higher binding affinity than the reference Orlistat through optimized van der Waals interactions (−59.90 kcal/mol) while maintaining favorable electrostatic contributions and manageable conformational strain. The structural analysis confirmed that octyl piperate achieves binding stabilization after approximately 70 ns with sustained contact occupancy of 6–12 interactions per frame, driven by favorable hydrophobic interactions with key residues Val329, Ala212, and Phe209.

Dodecyl piperate demonstrated substantial binding affinity (−68.26 kcal/mol) but with increased conformational flexibility and strain, suggesting that chain lengths beyond C8 may encounter diminishing returns due to entropic penalties despite enhanced hydrophobic contacts.

Interestingly, recent literature aligns well with our findings. For example, novel pancreatic lipase peptide inhibitors from yak milk cheese (RK7, KQ7) were characterized using molecular docking and showed enzymatic inhibition with an IC_{50} of 0.6 mg/mL [60]. Similarly, the stable binding of natural polyphenols, such as pinoresinol and ε-viniferin, to the pancreatic lipase active site was demonstrated using both computational and in vitro evidence [61]. The 3D-QSAR and MD study prioritized Chrysin as potent pancreatic lipase inhibitor over Genistein and Naringenin, reinforcing the importance of hydrophobic and H-bond in the interaction ligand-enzyme [62]. Furthermore, bromhexine was found to be a potential lipase inhibitor with mixed-mode inhibition and docking-supported binding pose stability [63].

4. Conclusions

In conclusion, the analysis reveals that hydrophobic optimization represents a highly effective strategy for lipase inhibitor design. The excellent correlation between docking predictions, MD simulation results, and experimental IC50 values validates our integrative approach and highlights octyl piperate as a promising candidate for the development of novel lipase inhibitors with potential applications in food preservation and antifungal therapy.

Supplementary Materials: The following supporting information can be downloaded at: https://www.mdpi.com/article/10.3390/reactions7010019/s1, Figure S1: HPLC analysis of piperate esters after 15 min of the inhibition reaction. Figure S2: Piperic acid simulation interactions diagram report. Figure S3: Butyl piperate simulation interactions diagram report. Figure S4: Octyl piperate simulation interactions diagram report. Figure S5: Dodecyl piperate simulation interactions diagram report. Figure S6: Orlistat simulation interactions diagram report.

Author Contributions: Conceptualization, A.F. and A.S.; methodology, A.M. and N.T.; software, N.T.; formal analysis, A.M.; investigation, A.M.; data curation, A.M.; writing—original draft preparation, A.M. and N.T.; writing—review and editing, O.A.A., A.F. and A.S.; supervision, A.F. and A.S.; project administration, A.S.; All authors have read and agreed to the published version of the manuscript.

Funding: This work was financially supported by the Ministry of Higher Education and Scientific Research in Tunisia through a grant to the Laboratory of Biochemistry and Enzymatic Engineering of Lipases—Ecole Nationale d'Ingénieurs de Sfax (ENIS).

Data Availability Statement: The original contributions presented in this study are included in the article/Supplementary Materials.

Conflicts of Interest: The authors declare no conflicts of interest.

References

1. Mahfoudhi, A.; Benmabrouk, S.; Fendri, A.; Sayari, A. Fungal Lipases as Biocatalysts: A Promising Platform in Several Industrial Biotechnology Applications. *Biotechnol. Bioeng.* **2022**, *119*, 3370–3392. [CrossRef]
2. Riaz, U.; Hassan, A.; Fatima, M.; Aziz, H.; Rasool, M.; Murtaza, G. Plant Secondary Metabolites and Environmental Stress: An Overview. In *Biology and Biotechnology of Environmental Stress Tolerance in Plants*; Roychoudhury, A., Ed.; Apple Academic Press: Palm Bay, FL, USA, 2023; pp. 1–23.
3. Higaki, S. Lipase Inhibitors for the Treatment of Acne. *J. Mol. Catal. B Enzym.* **2003**, *22*, 377–384. [CrossRef]
4. Sayari, A.; Mahfoudhi, A.; Alghamdi, O.A.; Hmida-Sayari, A. Characterization of Some Plant Extracts, Piperine, and Piperic Acid and Their Anti-Obesity and Anti-Acne Effects Through the In Vitro Inhibition of Pancreatic and Bacterial Lipases. *Catalysts* **2024**, *14*, 776. [CrossRef]
5. Elshafie, H.S.; Camele, I.N.; Mohamed, A.A. A Comprehensive Review on the Biological, Agricultural and Pharmaceutical Properties of Secondary Metabolites Based-Plant Origin. *Int. J. Mol. Sci.* **2023**, *24*, 3266. [CrossRef] [PubMed]
6. Hadrich, F.; Cher, S.; Gargouri, Y.T.; Adel, S. Antioxidant and Lipase Inhibitory Activities and Essential Oil Composition of Pomegranate Peel Extracts. *J. Oleo Sci.* **2014**, *63*, 515–525. [CrossRef] [PubMed]
7. Ahmad, A.; Hassan, S.W.; Banat, F. An Overview of Microalgae Biomass as a Sustainable Aquaculture Feed Ingredient: Food Security and Circular Economy. *Bioengineered* **2022**, *13*, 9521–9547. [CrossRef]
8. Mudgil, P.; Kamal, H.; Yuen, G.C.; Maqsood, S. Characterization and Identification of Novel Antidiabetic and Anti-Obesity Peptides from Camel Milk Protein Hydrolysates. *Food Chem.* **2018**, *259*, 46–54. [CrossRef] [PubMed]
9. Grundy, M.M.-L.; Edwards, C.H.; Mackie, A.R.; Gidley, M.J.; Butterworth, P.J.; Ellis, P.R. Re-Evaluation of the Mechanisms of Dietary Fibre and Implications for Macronutrient Bioaccessibility, Digestion and Postprandial Metabolism. *Br. J. Nutr.* **2016**, *116*, 816–833. [CrossRef]
10. Duda-Chodak, A.; Tarko, T. Possible Side Effects of Polyphenols and Their Interactions with Medicines. *Molecules* **2023**, *28*, 2536. [CrossRef]
11. Rajan, L.; Palaniswamy, D.; Mohankumar, S.K. Targeting Obesity with Plant-Derived Pancreatic Lipase Inhibitors: A Comprehensive Review. *Pharmacol. Res.* **2020**, *155*, 104681. [CrossRef]
12. Sharma, N.; Sharma, V.K.; Seo, S.-Y. Screening of Some Medicinal Plants for Anti-Lipase Activity. *J. Ethnopharmacol.* **2005**, *97*, 453–456. [CrossRef] [PubMed]
13. Jamai, K.; Daoudi, N.E.; Elrherabi, A.; Bnouham, M. Medicinal Plants and Natural Products to Treat Obesity through Inhibiting Pancreatic Lipase: A Review (2020–2022). *Lett. Drug Des. Discov.* **2023**, *21*, 1936–1955. [CrossRef]
14. Bustos, A.-S.; Håkansson, A.; Linares-Pastén, J.A.; Nilsson, L. Interaction between Myricetin Aggregates and Lipase under Simplified Intestinal Conditions. *Foods* **2020**, *9*, 777. [CrossRef]
15. Barrios-Nolasco, A.; Domínguez-López, A.; Miliar-García, Á.; Cornejo-Garrido, J.; Jaramillo-Flores, M.E. Anti-Inflammatory Effect of Ethanolic Extract from Tabebuia Rosea (Bertol.) DC., Quercetin, and Anti-Obesity Drugs in Adipose Tissue in Wistar Rats with Diet-Induced Obesity. *Molecules* **2023**, *28*, 3801. [CrossRef]
16. Ruiz, C.; Falcocchio, S.; Xoxi, E.; Villo, L.; Nicolosi, G.; Pastor, F.I.J.; Diaz, P.; Saso, L. Inhibition of Candida Rugosa Lipase by Saponins, Flavonoids and Alkaloids. *J. Mol. Catal. B Enzym.* **2006**, *40*, 138–143. [CrossRef]
17. Mahfoudhi, A.; Mabrouk, S.B.; Hadrich, B.; Mhadhbi, M.; Abderrazak, H.; Alghamdi, O.A.; Fendri, A.; Sayari, A. Efficient Green Enzymatic Synthesis of Lipophilic Piperic Acid Esters by Immobilized *Rhizopus Oryzae* Lipase: Optimization and Antioxidant Activities. *Catal. Lett.* **2024**, *154*, 4283–4301. [CrossRef]
18. Arifian, H.; Maharani, R.; Megantara, S.; Gazzali, A.M.; Muchtaridi, M. Amino-Acid-Conjugated Natural Compounds: Aims, Designs and Results. *Molecules* **2022**, *27*, 7631. [CrossRef]
19. Ben Salah, A.; Fendri, K.; Gargouri, Y. La Lipase de *Rhizopus oryzae*: Production, Purification et Caractéristiques Biochimiques. *Rev. Fr. Corps Gras* **1994**, *41*, 133–137.
20. Vipin, V.C.; Sebastian, J.; Muraleedharan, C.; Santhiagu, A. Enzymatic Transesterification of Rubber Seed Oil Using *Rhizopus Oryzae* Lipase. *Procedia Technol.* **2016**, *25*, 1014–1021. [CrossRef]
21. López-Fernández, J.; Benaiges, M.D.; Valero, F. *Rhizopus oryzae* Lipase, a Promising Industrial Enzyme: Biochemical Characteristics, Production and Biocatalytic Applications. *Catalysts* **2020**, *10*, 1277. [CrossRef]
22. Eskandari, A.; Leow, T.C.; Rahman, A.; Oslan, S.N. Recent Insight into the Advances and Prospects of Microbial Lipases and Their Potential Applications in Industry. *Int. Microbiol.* **2024**, *27*, 1597–1631. [CrossRef]
23. Kotogán, A.; Furka, Z.T.; Kovács, T.; Volford, B.; Papp, D.A.; Varga, M.; Huynh, T.; Szekeres, A.; Papp, T.; Vágvölgyi, C.; et al. Hydrolysis of Edible Oils by Fungal Lipases: An Effective Tool to Produce Bioactive Extracts with Antioxidant and Antimicrobial Potential. *Foods* **2022**, *11*, 1711. [CrossRef]

24. Chen, V.B.; Arendall, W.B.; Headd, J.J.; Keedy, D.A.; Immormino, R.M.; Kapral, G.J.; Murray, L.W.; Richardson, J.S.; Richardson, D.C. MolProbity: All-Atom Structure Validation for Macromolecular Crystallography. *Acta Crystallogr. D Biol. Crystallogr.* **2009**, *66*, 12–21. [CrossRef]
25. Alshehri, W.A.; Alghamdi, N.H.; Khalel, A.F.; Almalki, M.H.; Hadrich, B.; Sayari, A. Thermostable $CaCO_3$-Immobilized Bacillus Subtilis Lipase for Sustainable Biodiesel Production from Waste Cooking Oil. *Catalysts* **2024**, *14*, 253. [CrossRef]
26. Horchani, H.; Bouaziz, A.; Gargouri, Y.; Sayari, A. Immobilized Staphylococcus Xylosus Lipase-Catalysed Synthesis of Ricinoleic Acid Esters. *J. Mol. Catal. B Enzym.* **2012**, *75*, 35–42. [CrossRef]
27. Bouaziz, A.; Horchani, H.; Salem, N.B.; Chaari, A.; Chaabouni, M.; Gargouri, Y.; Sayari, A. Enzymatic Propyl Gallate Synthesis in Solvent-Free System: Optimization by Response Surface Methodology. *J. Mol. Catal. B Enzym.* **2010**, *67*, 242–250. [CrossRef]
28. Elgharbawy, A.A.; Riyadi, F.A.; Alam, M.Z.; Moniruzzaman, M. Ionic Liquids as a Potential Solvent for Lipase-Catalysed Reactions: A Review. *J. Mol. Liq.* **2018**, *251*, 150–166. [CrossRef]
29. Kumar, A.; Dhar, K.; Kanwar, S.S.; Arora, P.K. Lipase Catalysis in Organic Solvents: Advantages and Applications. *Biol. Proced. Online* **2016**, *18*, 2. [CrossRef] [PubMed]
30. Sandoval, G. Hydrolases and Their Application in Asymmetric Synthesis. In *Biocatalysis in Asymmetric Synthesis*; Elsevier: Amsterdam, The Netherlands, 2024; pp. 133–174. [CrossRef]
31. Mishra, S.; Kapoor, N.; Mubarak Ali, A.; Pardhasaradhi, B.V.V.; Kumari, A.L.; Khar, A.; Misra, K. Differential Apoptotic and Redox Regulatory Activities of Curcumin and Its Derivatives. *Free Radic. Biol. Med.* **2005**, *38*, 1353–1360. [CrossRef]
32. Zarai, Z.; Boujelbene, E.; Ben Salem, N.; Gargouri, Y.; Sayari, A. Antioxidant and Antimicrobial Activities of Various Solvent Extracts, Piperine and Piperic Acid from Piper Nigrum. *LWT–Food Sci. Technol.* **2013**, *50*, 634–641. [CrossRef]
33. Varadi, M.; Anyango, S.; Deshpande, M.; Nair, S.; Natassia, C.; Yordanova, G.; Yuan, D.; Stroe, O.; Wood, G.; Laydon, A.; et al. AlphaFold Protein Structure Database: Massively Expanding the Structural Coverage of Protein-Sequence Space with High-Accuracy Models. *Nucleic Acids Res.* **2022**, *50*, 439–444. [CrossRef] [PubMed]
34. Laskowski, R.A.; MacArthur, M.W.; Moss, D.S.; Thornton, J.M. PROCHECK: A Program to Check the Stereochemical Quality of Protein Structures. *J. Appl. Crystallogr.* **1993**, *26*, 283–291. [CrossRef]
35. Wiederstein, M.; Sippl, M.J. ProSA-Web: Interactive Web Service for the Recognition of Errors in Three-Dimensional Structures of Proteins. *Nucleic Acids Res.* **2007**, *35*, W407–W410. [CrossRef] [PubMed]
36. Colovos, C.; Yeates, T.O. Verification of Protein Structures: Patterns of Nonbonded Atomic Interactions. *Protein Sci.* **1993**, *2*, 1511–1519. [CrossRef]
37. Eisenberg, D.; Lüthy, R.; Bowie, J.U. VERIFY3D: Assessment of Protein Models with Three-Dimensional Profiles. *Methods Enzymol.* **1997**, *277*, 396–404. [CrossRef]
38. Sahayarayan, J.J.; Rajan, K.S.; Vidhyavathi, R.; Nachiappan, M.; Prabhu, D.; Alfarraj, S.; Arokiyaraj, S.; Daniel, A.N. In-Silico Protein-Ligand Docking Studies against the Estrogen Protein of Breast Cancer Using Pharmacophore Based Virtual Screening Approaches. *Saudi J. Biol. Sci.* **2021**, *28*, 400–407. [CrossRef]
39. Lu, C.; Wu, C.; Ghoreishi, D.; Chen, W.; Wang, L.; Damm, W.; Ross, G.A.; Dahlgren, M.K.; Russell, E.; Von Bargen, C.D.; et al. OPLS4: Improving Force Field Accuracy on Challenging Regimes of Chemical Space. *J. Chem. Theory Comput.* **2021**, *17*, 4291–4300. [CrossRef]
40. Oluwamodupe, C.; Babalola, O.O.; Ottu, P.O.; Aladeteloye, E.T.; Mogaji, E.T.; Olumodeji, E.O.; Adekanle, V.R.; Elekofehinti, O.O. The Inhibitory Effects of Centella Asiatica Compounds on Myeloid Cell Leukemia 1 (MCL-1) in Cancer: A Computational Study. *In Silico Pharmacol.* **2025**, *13*, 111. [CrossRef] [PubMed]
41. Derewenda, U.; Swenson, L.; Wei, Y.; Green, R.; Kobos, P.M.; Joerger, R.; Haas, M.J.; Derewenda, Z.S. Conformational Lability of Lipases Observed in the Absence of an Oil-Water Interface: Crystallographic Studies of Enzymes from the Fungi Humicola Lanuginosa and Rhizopus Delemar. *J. Lipid Res.* **1994**, *35*, 524–534. [CrossRef]
42. Mellaoui, M.D.; Zaki, K.; Abbiche, K.; Imjjad, A.; Boutiddar, R.; Sbai, A.; Jmiai, A.; El Issami, S.; Lamsabhi, A.M.; Zejli, H. In Silico Anticancer Activity of Isoxazolidine and Isoxazolines Derivatives: DFT Study, ADMET Prediction, and Molecular Docking. *J. Mol. Struct.* **2024**, *1308*, 138330. [CrossRef]
43. Uba, A.I.; Hryb, M.; Singh, M.; Bui-Linh, C.; Tran, A.; Atienza, J.; Misbah, S.; Mou, X.; Wu, C. Discovery of Novel Inhibitors of Histone Deacetylase 6: Structure-Based Virtual Screening, Molecular Dynamics Simulation, Enzyme Inhibition and Cell Viability Assays. *Life Sci.* **2024**, *338*, 122395. [CrossRef] [PubMed]
44. Brylinski, M. Aromatic Interactions at the Ligand-Protein Interface: Implications for the Development of Docking Scoring Functions. *Chem. Biol. Drug Des.* **2017**, *91*, 380–390. [CrossRef]
45. Onufriev, A.V.; Izadi, S. Water Models for Biomolecular Simulations. *WIREs Comput. Mol. Sci.* **2017**, *8*, e1347. [CrossRef]
46. Ke, Q.; Gong, X.; Liao, S.; Duan, C.; Li, L. Effects of Thermostats/Barostats on Physical Properties of Liquids by Molecular Dynamics Simulations. *J. Mol. Liq.* **2022**, *365*, 120116. [CrossRef]
47. Samaniego-Rojas, J.D.; Gaumard, R.; Alejandre, J.; Mineva, T.; Geudtner, G.; Köster, A.M. A Molecular Mechanics Implementation of the Cyclic Cluster Model. *Z. Naturforsch. B* **2024**, *79*, 201–213. [CrossRef]

48. Wells, B.A.; Chaffee, A.L. Ewald Summation for Molecular Simulations. *J. Chem. Theory Comput.* **2015**, *11*, 3684–3695. [CrossRef] [PubMed]
49. Kottekad, S.; Roy, S.; Dandamudi, U. A Computational Study to Probe the Binding Aspects of Potent Polyphenolic Inhibitors of Pancreatic Lipase. *J. Biomol. Struct. Dyn.* **2023**, *42*, 3472–3491. [CrossRef] [PubMed]
50. Moreno, D.A.; Ilic, N.; Poulev, A.; Brasaemle, D.L.; Fried, S.K.; Raskin, I. Inhibitory Effects of Grape Seed Extract on Lipases. *Nutrition* **2003**, *19*, 876–879. [CrossRef]
51. Jumper, J.; Evans, R.; Pritzel, A.; Green, T.; Figurnov, M.; Ronneberger, O.; Tunyasuvunakool, K.; Bates, R.; Žídek, A.; Potapenko, A.; et al. Highly Accurate Protein Structure Prediction with AlphaFold. *Nature* **2021**, *596*, 583–589. [CrossRef]
52. Terwilliger, T.C.; Liebschner, D.; Croll, T.I.; Williams, C.J.; McCoy, A.J.; Poon, B.K.; Afonine, P.V.; Oeffner, R.D.; Richardson, J.S.; Read, R.J.; et al. AlphaFold Predictions Are Valuable Hypotheses and Accelerate but Do Not Replace Experimental Structure Determination. *Nat. Methods* **2024**, *21*, 110–116. [CrossRef]
53. Tan, L.H.; Kwoh, C.K.; Mu, Y. RmsdXNA: RMSD Prediction of Nucleic Acid-Ligand Docking Poses Using Machine-Learning Method. *Brief. Bioinform.* **2024**, *25*, bbae166. [CrossRef] [PubMed]
54. da Fonseca, A.M.; Caluaco, B.J.; Martinho, J.; Cabongo, S.Q.; Gaieta, E.M.; Djata, F.; Colares, R.P.; Freire, C.; Freire, C.; Neto, M.M.; et al. Screening of Potential Inhibitors Targeting the Main Protease Structure of SARS-CoV-2 via Molecular Docking, and Approach with Molecular Dynamics, RMSD, RMSF, H-Bond, SASA and MMGBSA. *Mol. Biotechnol.* **2023**, *66*, 1919–1933. [CrossRef]
55. Bian, Y.; Zhang, Y.; Wang, T.; Yang, C.; Feng, Z.; Goh, K.-L.; Zhou, Y.; Zheng, M. Insights into the Enzymatic Synthesis of Alcoholic Flavor Esters with Molecular Docking Analysis. *LWT–Food Sci. Technol.* **2024**, *200*, 116206. [CrossRef]
56. Zhang, T.; Zhang, Y.; Deng, C.; Zhong, H.; Gu, T.; Goh, K.-L.; Han, Z.; Zheng, M.; Zhou, Y. Green and Efficient Synthesis of Highly Liposoluble and Antioxidant L-Ascorbyl Esters by Immobilized Lipases. *J. Clean. Prod.* **2022**, *379*, 134772. [CrossRef]
57. Sankar, V.; Maida Engels, S.E. Synthesis, Biological Evaluation, Molecular Docking and in Silico ADME Studies of Phenacyl Esters of N-Phthaloyl Amino Acids as Pancreatic Lipase Inhibitors. *Future J. Pharm. Sci.* **2018**, *4*, 276–283. [CrossRef]
58. Dahabiyeh, L.A.; Bustanji, Y.; Taha, M.O. The Herbicide Quinclorac as Potent Lipase Inhibitor: Discovery via Virtual Screening and in Vitro/in Vivo Validation. *Chem. Biol. Drug Des.* **2018**, *93*, 787–797. [CrossRef]
59. Singh, A.P.; Arya, H.; Singh, V.; Kumar, P.; Gautam, H.K. Identification of Natural Inhibitors to Inhibit C. Acnes Lipase through Docking and Simulation Studies. *J. Mol. Model.* **2022**, *28*, 281. [CrossRef] [PubMed]
60. Wang, P.; Song, X.; Liang, Q. Molecular Docking Studies and In Vitro Activity of Pancreatic Lipase Inhibitors from Yak Milk Cheese. *Int. J. Mol. Sci.* **2025**, *26*, 756. [CrossRef]
61. Citriniti, E.L.; Rocca, R.; Sciacca, C.; Cardullo, N.; Muccilli, V.; Ortuso, F.; Alcaro, S. Leveraging Natural Compounds for Pancreatic Lipase Inhibition via Virtual Screening. *Pharmaceuticals* **2025**, *18*, 1246. [CrossRef] [PubMed]
62. Zhai, Y.; Wang, K.; Yu, Z.; Zhou, S.; Fan, J. Pancreatic Lipase Inhibitors: Virtual Screening and Mechanistic Analysis. *Int. J. Biol. Macromol.* **2025**, *310*, 143128. [CrossRef]
63. Gholami, A.; Minai-Tehrani, D.; Eriksson, L.A. Combining Kinetics and in Silico Approaches to Evaluate Bromhexine as an Anti-Pancreatic Lipase Agent for Obesity Management. *Sci. Rep.* **2025**, *15*, 18420. [CrossRef] [PubMed]

Disclaimer/Publisher's Note: The statements, opinions and data contained in all publications are solely those of the individual author(s) and contributor(s) and not of MDPI and/or the editor(s). MDPI and/or the editor(s) disclaim responsibility for any injury to people or property resulting from any ideas, methods, instructions or products referred to in the content.